COMMUNICATION

Check for updates

An ester electrolyte for lithium–sulfur batteries capable of ultra-low temperature cycling†

Guorui Cai,[a] John Holoubek,[a] Dawei Xia,[a] Mingqian Li,[b] Yijie Yin,[c] Xing Xing,[c] Ping Liu [ID] [abcd] and Zheng Chen [ID] *[abcd]

A novel lithium bis(fluorosulfonyl)imide in a methyl propionate/ fluoroethylene carbonate (LiFSI MP/FEC) electrolyte was designed for high compatibility with the Li metal and sulfurized polyacrylonitrile (SPAN). The resulting Li‖SPAN cells can charge and discharge at −20 °C and −40 °C with over 91% and 78% room temperature capacity retention.

The demand for rechargeable batteries with increased energy density at sub-zero temperatures is increasing, especially for portable devices in harsh environments such as high altitude, arctic regions, outer space, and abyss explorations.[1–3] However, state-of-the-art Li-ion batteries (LIBs) composed of graphite anodes (372 mA h g^{-1}) and lithium transition metal oxide cathodes cannot conceivably deliver >300 W h kg^{-1} at the cell level, which deteriorates even further under extremely cold conditions.[4,5]

To increase the energy density of LIBs, tremendous effort has been focused on the application of Li metal (3860 mA h g^{-1}), the highest-energy-density anode.[6,7] Additionally, abundantly available elemental sulfur, with a theoretical energy density of 2600 W h kg^{-1}, has also received attention as a next-generation cathode material.[8,9] Unfortunately, Li–S batteries have limitations such as less utilization of active materials and poor cycling performance, which are caused by the electronically insulating nature of sulfur, the shuttling of soluble polysulfide intermediates, and the instability of the Li anode. As an alternative solution, Li–S batteries based on sulfur composites, such as sulfurized polyacrylonitrile (SPAN),[10–16] have been found to effectively overcome some of the problems associated with sulfur electrodes. Despite the high compatibility of SPAN with carbonate-based electrolytes, practical cells typically fail to achieve stable long-term cycling due to the poor Li metal stability found in such electrolytes.[10–16]

Furthermore, the high melting point of carbonate electrolytes further limits the application of Li–SPAN batteries at low temperatures. To preserve the energy output, numerous reports have been focused on the development of low-temperature electrolytes to increase the ionic conductivity and reduce the charge transfer resistance of the current LIBs.[17–26] Carboxylate ester-based co-solvents with low melting points and viscosity are commonly employed to do so.[21–25] However, these molecules display high reactivity with the Li metal, resulting in reduced cycling performance and hazardous dendrite growth, especially at extremely cold temperatures.[27] To improve the performance of such carboxylate ester-containing electrolytes, fluoride-donating additives were introduced in previous studies for the production of fluorine-rich solid electrolyte interphase (SEI) layers to improve the cycling performance of the Li metal anode, which simultaneously provided the Li metal anode with improved reversibility and sub-zero temperature performance.[23–25] However, to the best of our knowledge, the use of electrolytes that simultaneously improve the lithium metal and sulfur-based cathodes at extremely low-temperatures remains a significant challenge.

Herein, a new ester-based electrolyte is developed for Li–SPAN batteries capable of cycling at ultra-low temperatures, in which methyl propionate (MP), a common carboxylate ester with a low melting point (−87.5 °C) and a suitable dielectric constant (6.23), is used as the primary solvent. Fluoroethylene carbonate (FEC, 10% by volume) and lithium bis(fluorosulfonyl)imide (LiFSI, 1 M) are applied as a co-solvent additive and Li salt, respectively, both of which are known to stabilize the SEI.[10,12,13,23–26] As a result, this LiFSI MP/FEC electrolyte system exhibits high compatibility with both the Li metal anode and the SPAN cathode, and thus provides high room temperature capacity retention (>78%) and cycling stability (capacity fade < 0.14% per cycle) even at −40 °C.

[a] Department of NanoEngineering, University of California, San Diego, La Jolla, CA 92093, USA. E-mail: zhengchen@eng.ucsd.edu; Web: http://zhengchen.eng.ucsd. edu/

[b] Program of Chemical Engineering, University of California, San Diego, La Jolla, CA 92093, USA

[c] Program of Materials Science, University of California, San Diego, La Jolla, CA 92093, USA

[d] Sustainable Power and Energy Center, University of California, San Diego, La Jolla, CA 92093, USA

† Electronic supplementary information (ESI) available: Material synthesis and fabrication, and supplementary figures. See DOI: 10.1039/d0cc03798b
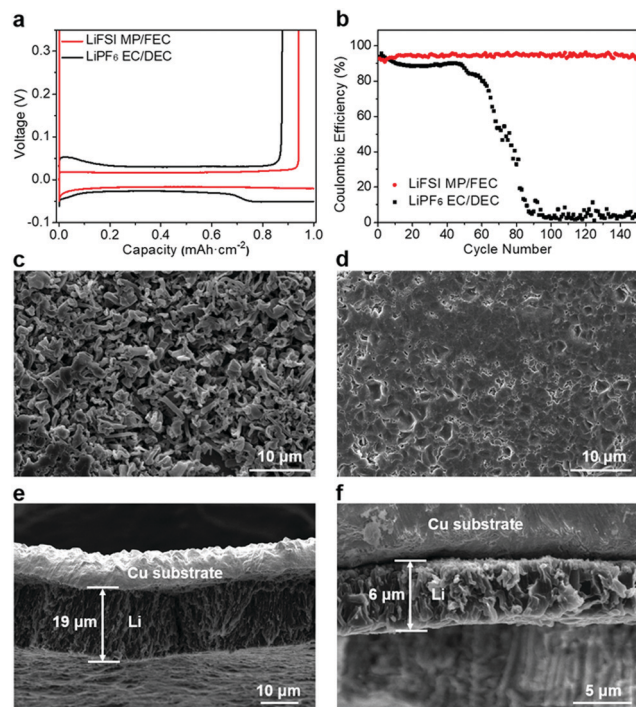
Fig. 1 Li metal performance in the selected electrolytes at room temperature. (a) Li plating/stripping curves and (b) long-term cycling performance of Li||Cu cells in LiFSI MP/FEC, and LiPF$_6$ EC/DEC at 0.5 mA cm^{-2}; top (c and d) and cross-section (e and f) views of the SEM images of Li deposits obtained in LiPF$_6$ EC/DEC (c and e) and LiFSI MP/FEC (d and f) at 1 mA h cm^{-2} and 0.5 mA cm^{-2}.

In order to investigate the compatibility of the LiFSI MP/FEC electrolyte with the Li metal anode, Li||Cu cells with different electrolytes were assembled. The industry-type 1 M LiPF$_6$ in the ethylene carbonate/diethyl carbonate (EC/DEC, 1:1 in volume) electrolyte was selected as the control electrolyte due to a large volume of published studies conducted with similar formulations in this research field.[10–15] As shown in Fig. 1a, the LiFSI MP/FEC electrolyte provides smooth plating/stripping curves with a significantly higher Coulombic efficiency (CE) than the LiPF$_6$ EC/DEC system (94.2% vs. 88.3%), indicating that the former exhibits higher compatibility with the Li metal anode. This trend is further supported by the long-term cycling performance (Fig. 1b), in which LiFSI MP/FEC retains a CE of 93.4% after 150 cycles. In contrast, the CE of the industry-type electrolyte system shows a sharp decrease after 50 cycles, as a result of the continuous formation of porous inactive Li and depletion of the electrolyte.[28–30] To further compare their Li plating behavior, the Li||Cu cells after plating 1 mA h cm^{-2} of Li at 0.5 mA cm^{-2} were disassembled and the morphology of the plated Li was examined by scanning electron microscopy (SEM), in which the LiPF$_6$ EC/DEC system produced a highly dendritic Li structure (Fig. 1c), a common phenomenon for similar electrolyte systems with poor reductive stability towards the Li metal.[24,27,28] The LiFSI MP/FEC electrolyte system, on the other hand, exhibited large Li chunks without noticeable dendrites (Fig. 1d). Based on the cross-section views of the SEM images (Fig. 1e and f), the plated Li in the LiPF$_6$ EC/DEC
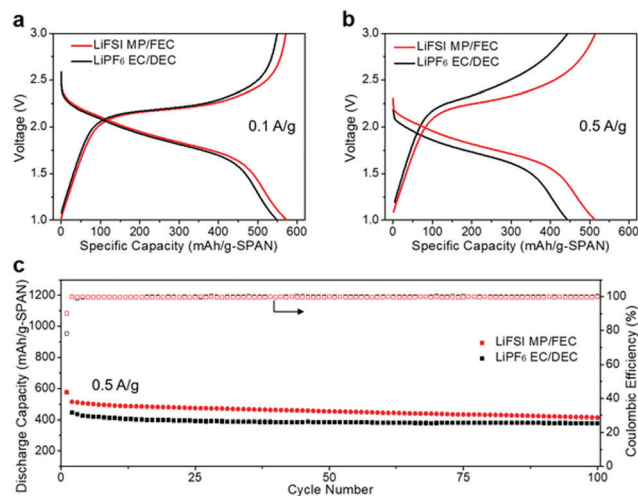

Fig. 2 Li||SPAN half-cell performance in different electrolytes at room temperature. Voltage curves at (a) 0.1 A g^{-1} and (b) 0.5 A g^{-1}; (c) long-term cycling performance at 0.5 A g^{-1}.

electrolyte exhibited a thickness of ∼19 μm, whereas the plated Li in the LiFSI MP/FEC electrolyte presented a dense structure with a thickness of ∼6 μm, close to the calculated theoretical thickness of 4.8 μm, which indicates a low porosity (∼20%), and thus minimizes the Li surface area and its parasitic reactions with the electrolyte.[28–30] Therefore, all the above results indicate the superiority of the LiFSI MP/FEC system for Li metal anode stability.

To test the effect of these electrolytes on the performance of the SPAN cathode, the Li||SPAN half cells were assembled. As observed in Fig. 2a and b, the LiFSI MP/FEC system provides typical charge–discharge curves commonly observed in carboxylate ester-based electrolyte systems.[10–15] In addition, long-term cycling tests demonstrated that the LiFSI MP/FEC system has a capacity retention of 81% after 100 cycles, as well as a CE of ∼99.9% at 0.5 A g^{-1}, indicating that SPAN has negligible dissolution and shuttling in the LiFSI MP/FEC system (Fig. 2b and Fig. S1, ESI†).[25]

To demonstrate the advantage of the LiFSI MP/FEC electrolyte at sub-zero temperature, after activation at room temperature for two cycles, the Li||SPAN half cells were cycled at −20 and −40 °C. The corresponding voltage profiles at 0.1 A g^{-1} are displayed in Fig. 3a and b. Although both electrolyte systems show comparable capacity and cycling stability at room temperature (Fig. 2a and c), the capacity retention of these cells with the industry-type carbonate electrolyte suffers from a dramatic fade of both the operating voltage and capacity with a decrease of the testing temperature. In particular at −40 °C (Fig. 3b), the LiPF$_6$ EC/DEC electrolyte system retained less than 1% of its room temperature capacity, a result similar to those reported in our previous studies, attributed to the strong binding between Li$^+$ and EC, as well as the high melting point of the EC/DEC solvent.[24] On the contrary, the LiFSI MP/FEC electrolyte system is superior in the above aspects, in which the low melting point of MP ensures high retention of ionic conductivity at extremely cold temperatures, and the replacement of EC with FEC allows for a facile de-solvation process due to the significantly weaker Li$^+$ binding
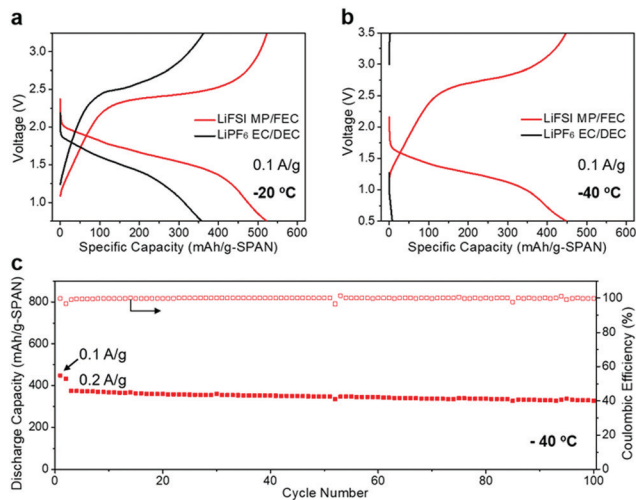
Fig. 3 Li||SPAN half cell performance at ultra-low temperatures. Voltage curves of Li||SPAN cells at (a) −20 °C and (b) −40 °C with a current density of 0.1 A g⁻¹ in each electrolyte; (c) long-term cycling performance of Li||SPAN half cells charging and discharging at −40 °C in LiFSI MP/FEC.

Fig. 4 Electrochemical behavior of the selected electrolytes in Li||SPAN half cells and Li||Li and SPAN||SPAN symmetrical cells at different temperatures. Nyquist plots of (a) Li||SPAN half cells, (b) Li||Li symmetrical cells, and (c) SPAN||SPAN cells at 25 °C, −20 °C, and −40 °C in LiFSI MP/FEC; (d) voltage curves of Li||Cu cells at 25 °C, −20 °C, and −40 °C in LiFSI MP/FEC at 0.15 mA cm⁻² and 1 mA h cm⁻².

energy of FEC.[24] As a result, the MP/FEC system was able to offer a 91% and 78% room-temperature capacity retention at 0.1 A g⁻¹, −20 °C and −40 °C, respectively (Fig. 2a and 3a, b). To further highlight their ability to work at ultra-low temperatures, the long-term cycling of the Li–SPAN half cells was conducted at −20 and −40 °C (Fig. 3c and Fig. S2, ESI†), where over 86% of the initial capacity was retained for 100 cycles at 0.2 A g⁻¹.

To better understand the performance of these Li||SPAN cells at extremely low temperatures, further electrochemical characterization was performed. Electrochemical impedance spectroscopy (EIS) of 50% state of charge (SOC) symmetric positive electrode cells was applied in addition to EIS of Li||Li and Li||SPAN cells to deconvolute the respective impedance contributions.[23] It was observed that the Li||SPAN cells exhibited charge transfer impedances of 75, 1140, and 7762 Ω at 25, −20, and −40 °C, respectively, far beyond the bulk ionic resistance (∼3, 6, and 12 Ω). In order to probe the anode and cathode sides, a symmetric Li||Li cell and a SPAN||SPAN cell at 50% SOC were analysed under the same conditions (Fig. 4a–c). Although both the anode and cathode sides exhibited a small charge transfer impedance at room temperature (16 and 55 Ω), the Li metal side provides consistently higher impedance than the SPAN cathode at sub-zero temperatures, producing charge transfer impedances of 2126 and 15 470 Ω compared to only 737 and 5280 Ω at −20 and −40 °C, respectively. This resistance trend for the Li anode was also investigated in the Li||Cu cells at 0.15 mA cm⁻². As shown in Fig. 4d, the Li||Cu cells provide ∼0.007 V, 0.25 V, and 0.60 V overpotential at room temperature, −20 °C and −40 °C, respectively. Their increased overpotentials at low temperatures (−20 °C and −40 °C) in comparison with those at room temperature share the same trend as those with the Li||SPAN half cells (∼0.24 V and 0.59 V *vs.* ∼0.26 V and 0.61 V), indicating that the rapidly increased impedance on the anode side is the main reason for the reduced capacity of the Li||SPAN half cells at ultra-low temperatures. The corresponding

data in the LiPF₆ EC/DEC (Fig. S3–S5, ESI†) electrolyte system also exhibited the same trend as the above results, but this electrolyte system showed ∼300% higher impedance at ultra-low temperatures, which is consistent with the significantly lower capacity retention under these conditions (Fig. 3a and b).

In summary, a carboxylate ester-based electrolyte system for ultra-low temperature Li–SPAN batteries was developed, in which the main solvent MP ensures a low melting point, and the fluoride-donating FSI and FEC components improved the compatibility of MP with Li metal. Electrochemical results show that the LiFSI MP/FEC electrolyte can provide the Li||SPAN cells with higher Li metal compatibility (CE: 94.2% *vs.* 88.3% at room temperature) and long-term stability compared to the industry-type carbonate electrolyte at room and ultra-low temperatures due to the improved compatibility with both Li metal anodes and SPAN cathodes. When cycled at a current density of 0.1 A g⁻¹, the Li||SPAN half cells retained over 91% and 78% of their room temperature capacity at −20 °C and −40 °C, respectively. The Li–SPAN cells also retained 86% of their initial capacity at 0.2 A g⁻¹ after 100 cycles at −40 °C. Different from the strategies used to preserve the energy output of LIBs,[3,24,31,32] this work provides a crucial design strategy for rechargeable batteries with high energy density at ultra-low temperatures by simultaneously increasing the baseline energy density of the batteries and lowering the energy loss at sub-zero temperatures.

Conflicts of interest

There are no conflicts to declare.

Notes and references

1 M. C. Smart, B. V. Ratnakumar, R. C. Ewell, S. Surampudi, F. J. Puglia and R. Gitzendanner, *Electrochim. Acta*, 2018, **268**, 27–40.
2 K. B. Chin, E. J. Brandon, R. V. Bugga, M. C. Smart, S. C. Jones, F. C. Krause, W. C. West and G. G. Bolotin, *Proc. IEEE*, 2018, **106**, 419–728.
3 M.-T. F. Rodrigues, G. Babu, H. Gullapalli, K. Kalaga, F. N. Sayed, K. Kato, J. Joyner and P. M. Ajayan, *Nat. Energy*, 2017, **2**, 17108.
4 J. Jaguemont, L. Boulon and Y. Dubé, *Appl. Energy*, 2016, **164**, 99–114.
5 C. K. Huang, J. S. Sakamoto, J. Wolfenstine and S. Surampudi, *J. Electrochem. Soc.*, 2000, **147**, 2893–2896.
6 J. Liu, Z. Bao, Y. Cui, E. J. Dufek, J. B. Goodenough, P. Khalifah, Q. Li, B. Y. Liaw, P. Liu and A. Manthiram, *et al.*, *Nat. Energy*, 2019, **4**, 180–186.
7 X. Fan, L. Chen, O. Borodin, X. Ji, J. Chen, S. Hou, T. Deng, J. Zheng, C. Yang and S.-C. Liou, *et al.*, *Nat. Nanotechnol.*, 2018, **13**, 715–722.
8 Q. Pang, X. Liang, C. Y. Kwok and L. F. Nazar, *Nat. Energy*, 2016, **1**, 16132.
9 A. Gupta, A. Bhargav, J. P. Jones, R. V. Bugga and A. Manthiram, *Chem. Mater.*, 2020, **32**, 2070–2077.
10 H. Yang, J. Chen, J. Yang and J. Wang, *Angew. Chem., Int. Ed.*, 2020, **59**, 7306–7318.
11 J. Wang, Y. S. He and J. Yang, *Adv. Mater.*, 2015, **27**, 569–575.
12 W.-J. Chen, B.-Q. Li, C.-X. Zhao, M. Zhao, T.-Q. Yuan, R.-C. Sun, J.-Q. Huang and Q. Zhang, *Angew. Chem., Int. Ed.*, 2020, **59**, 10732–10745.
13 Z. Chen, J. Zhou, Y. Guo, C. Liang, J. Yang, J. Wang and Y. Nuli, *Electrochim. Acta*, 2018, **282**, 555–562.
14 Z. Xu, J. Wang, J. Yang, X. Miao, R. Chen, J. Qian and R. Miao, *Angew. Chem., Int. Ed.*, 2016, **55**, 10372–10375.
15 S. Wei, L. Ma, K. E. Hendrickson, Z. Tu and L. A. Archer, *J. Am. Chem. Soc.*, 2015, **137**, 12143–12152.
16 X. Xing, Y. Li, X. Wang, V. Petrova, H. Liu and P. Liu, *Energy Storage Mater.*, 2019, **21**, 474–480.
17 C. S. Rustomji, Y. Yang, T. K. Kim, J. Mac, Y. J. Kim, E. Caldwell, H. Chung and Y. S. Meng, *Science*, 2017, **356**, eaal4263.
18 X. Fan, X. Ji, L. Chen, J. Chen, T. Deng, F. Han, J. Yue, N. Piao, R. Wang and X. Zhou, *et al.*, *Nat. Energy*, 2019, **4**, 882–890.
19 Q. Li, S. Jiao, L. Luo, M. S. Ding, J. Zheng, S. S. Cartmell, C.-M. Wang, K. Xu, J.-G. Zhang and W. Xu, *ACS Appl. Mater. Interfaces*, 2017, **9**, 18826–18835.
20 S. S. Zhang, K. Xu, J. L. Allen and T. R. Jow, *J. Power Sources*, 2002, **110**, 216–221.
21 M. C. Smart, B. V. Ratnakumar, K. B. Chin and L. D. Whitcanack, *J. Electrochem. Soc.*, 2010, **157**, A1361–A1374.
22 X. Dong, Z. Guo, Z. Guo, Y. Wang and Y. Xia, *Joule*, 2018, **2**, 902–913.
23 J. Holoubek, Y. J. Yin, M. Q. Li, M. Y. Yu, Y. M. Meng, P. Liu and Z. Chen, *Angew. Chem., Int. Ed.*, 2019, **58**, 18892–18897.
24 J. Holoubek, M. Yu, S. Yu, M. Li, Z. Wu, D. Xia, P. Bhaladhare, M. S. Gonzalez, T. A. Pascal, P. Liu and Z. Chen, *ACS Energy Lett.*, 2020, **5**, 1438–1447.
25 M. C. Smart, B. L. Lucht, S. Dalavi, F. C. Krause and B. V. Ratnakumar, *J. Electrochem. Soc.*, 2012, **159**, A739–A751.
26 E. Markevich, G. Salitra and D. Aurbach, *ACS Energy Lett.*, 2017, **2**, 1337–1345.
27 A. C. Thenuwara, P. P. Shetty and M. T. McDowell, *Nano Lett.*, 2019, **19**, 8664–8672.
28 S. Chen, J. Zheng, D. Mei, K. S. Han, M. H. Engelhard, W. Zhao, W. Xu, J. Liu and J.-G. Zhang, *Adv. Mater.*, 2018, **30**, 1706102.
29 S. Li, M. Jiang, Y. Xie, H. Xu, J. Jia and J. Li, *Adv. Mater.*, 2018, **30**, 1706375.
30 C. Fang, J. Li, M. Zhang, Y. Zhang, F. Yang, J. Z. Lee, M.-H. Lee, J. Alvarado, M. A. Schroeder, Y. Yang, B. Lu, N. Williams, M. Ceja, L. Yang, M. Cai, J. Gu, K. Xu, X. Wang and Y. S. Meng, *Nature*, 2019, **572**, 511–515.
31 C.-Y. Wang, G. Zhang, S. Ge, T. Xu, Y. Ji, X.-G. Yang and Y. Leng, *Nature*, 2016, **529**, 515–518.
32 B. Liao, H. Li, M. Xu, L. Xing, Y. Liao, X. Ren, W. Fan, L. Yu, K. Xu and W. Li, *Adv. Energy Mater.*, 2018, **8**, 1800802.